Lithos 118 (2010) 50–60

Contents lists available at ScienceDirect

Lithos

journal homepage: www.elsevier.com/locate/lithos

A unique Mo deposit associated with carbonatites in the Qinling orogenic belt, central China

Cheng Xu [a,*], Jindrich Kynicky [b], Anton R. Chakhmouradian [c], Liang Qi [d], Wenlei Song [d]

[a] Laboratory of Orogenic Belts and Crustal Evolution, Peking University, Beijing 100871, China
[b] Department of Geology and Pedology, Mendel University of Agriculture and Forestry, Brno, Czech Republic
[c] Department of Geological Sciences, University of Manitoba, Winnipeg, Manitoba, Canada
[d] Institute of Geochemistry, Chinese Academy of Sciences, Guiyang 550002, China

ARTICLE INFO

Article history:
Received 27 November 2009
Accepted 9 March 2010
Available online 17 March 2010

Keywords:
Carbonatite
Molybdenite
REE minerals
Mo deposits
Mantle source
Huanglongpu

ABSTRACT

The Qinling molybdenum belt is a prominent metallogenic structure in central China hosting several significant porphyry- and porphyry–skarn-type deposits. The Huanglongpu Mo deposit in the north-western part of the belt is unique in that it is associated with carbonatite dykes, rather than felsic magmatism. The carbonatites are composed largely of Sr–Mn-rich calcite and characterized by high concentrations of Sr and rare-earth elements (REE), and stable-isotope values indicative of a mantle source ($\delta^{13}C_{PDB} = -6.7 \pm 0.2‰$ and $\delta^{18}O_{SMOW} = 8.2 \pm 1.0‰$). Molybdenite is associated with galena and REE minerals (parisite, bastnäsite and monazite). Both molybdenite and galena are characterized by high Re contents (up to 0.4 and 0.2 wt.%, respectively) and Re/(Mo, Pb) ratios approaching the primitive-mantle values. In contrast to the rock-forming calcite, the REE minerals are enriched in light REE, whose relative proportion increases from parisite-(Ce) [average $(La/Nd)_n = 2.1$] to bastnäsite-(Ce) and monazite-(Ce) [average $(La/Nd)_n = 3.1$, 4.6, respectively]. The whole-rock compositions are characterized by some of the highest Mo and heavy REE abundances reported for carbonatites to date: up to 1010 ppm Mo, 1130 ppm Y + Gd…Lu and $(La/Yb)_n = 1.2–2.7$. The unusual trace-element geochemistry of the Huanglongpu rocks may ultimately reflect the composition of their mantle source, but their enrichment in Mo + Re was undoubtedly enhanced through preferential partitioning of these elements into a light REE–Pb–S-rich fluid derived from the carbonatitic magma modified by calcite fractionation. The present work shows that Mo can be retained, transported and deposited by carbonatitic fluids capable of generating economic Mo deposits.

© 2010 Elsevier B.V. All rights reserved.

1. Introduction

The global molybdenum supply is derived almost exclusively from porphyry-type ore deposits, such as the famous Climax-type deposits in Colorado and New Mexico, USA (Carten et al., 1993; Klemm et al., 2008), Endako mine in the Canadian Cordillera (Villeneuve et al., 2001), and Qinling in China (Hu et al., 1988; Chen et al., 2000). These deposits are associated with shallow intrusions of granites and high-silica rhyolites, and form where magmatic–hydrothermal fluids are expelled by crystallizing magmas of felsic to intermediate composition in regions of plate convergence (Burnham, 1997; Xu et al., 1998). Cooling, depressurization and reaction of fluids with wall-rock cause metals to precipitate in and around fractures, forming veins accompanied by an alteration envelope. Owing to superposition of multiple mineralizing events, fluid inclusions that trapped fluids of different composition and age are commonly juxtaposed within a single vein. Such superposition obscures the textural and temporal relations between the fluid inclusions, primary minerals and alteration assemblages and, thus, complicates the interpretation of fluid origin and evolution (e.g., Seedorff and Einaudi, 2004a; Seedorff et al., 2005; Rusk et al., 2008). The current models for Mo porphyry mineralization are not entirely consistent with many of the complex geological characteristics of porphyry orebodies (Seedorff et al., 2008), and many aspects of the genesis of Mo mineralization remain poorly understood. In the East Qinling orogenic belt, this type of mineralization is associated with carbonatites and, thus, may provide important insights into Mo transport and deposition beyond felsic porphyry systems.

The Qinling area is an important metallogenic belt hosting Au, Ag, Pb–Zn, W and Sb deposits, as well as the most important Mo ore camp in China. Its total measured reserves amount to 50×10^5 t of Mo metal and include five world-class superlarge ($>5 \times 10^5$ t Mo), five large ($5–20 \times 10^4$ t Mo) and several medium and small ($<5 \times 10^4$ t Mo) deposits (Li et al., 2007; Mao et al., 2008). The majority of these deposits are hosted by granitic porphyry bodies, but some are transitional porphyry–skarn deposits (Zhang et al., in press). The Huanglongpu deposit is unique and unparalleled worldwide in that it is associated with carbonatites, rather than silica-oversaturated

* Corresponding author.
E-mail address: xucheng1999@hotmail.com (C. Xu).

0024-4937/$ – see front matter © 2010 Elsevier B.V. All rights reserved.
doi:10.1016/j.lithos.2010.03.013

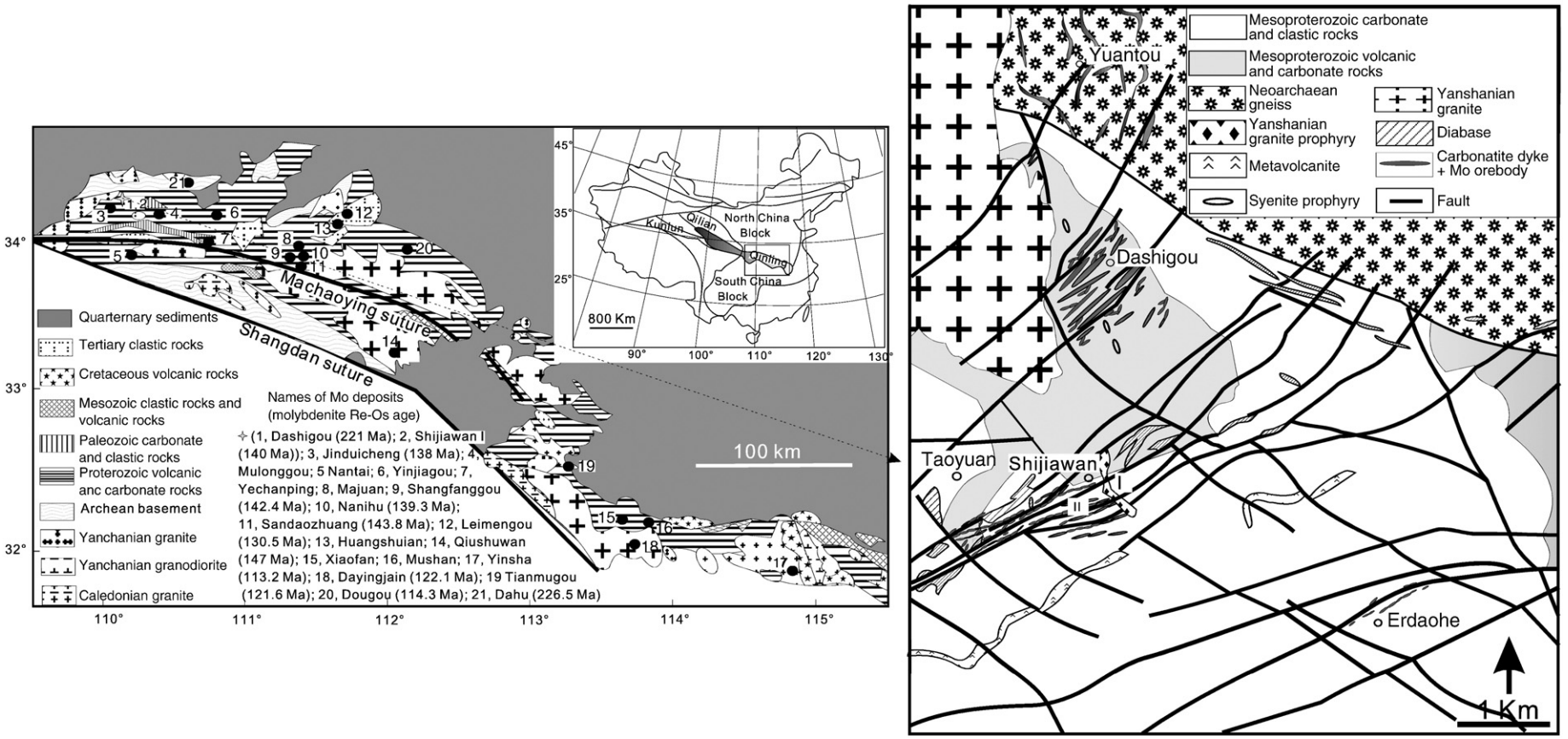

Fig. 1. Distribution of Mo deposits in the Qinling orogenic belt and geological sketch of the Hunaglongpu deposit (modified after Geological Team no. 13, 1989; Li et al., 2007; Mao et al., 2008).

igneous rocks. It is composed of four orefields with a total ore reserve of more than 0.18 million tons of MoS_2, making it a large Mo deposit. Almost all porphyry and porphyry–skarn deposits in the Qinling belt formed in the Late Jurassic–Early Cretaceous, as indicated by molybdenite Re–Os ages ranging from 148 to 112 Ma (Fig. 1; Huang et al., 1995; Mao et al., 2008), whereas molybdenite from the Huanglongpu deposit is much older, yielding a Re–Os age of 221 Ma (Huang et al., 1995; Stein et al., 1997). It is thus reasonable to expect that the old and petrologically unique carbonatite-hosted Mo deposit at Huanglongpu holds clues to the origin and early history of the large-scale Mo mineralization in the Qinling belt. However, there has been very little geochemical work done on the Huanglongpu deposit to date and its evolutionary history remains poorly understood. The present paper reports new data on the compositions of rocks and minerals from three of the four Mo orefields at Huanglongpu. The primary aim of the present work was to establish whether the Mo mineralization is genetically related to the carbonatites or derived from an external source.

2. Geological setting and sample provenance

2.1. Geology of the Qinling belt

The Qinling orogenic belt is divided into two parts, North Qinling and South Qinling, separated by the Shangdan suture (Fig. 1). The northern border of the North Qinling is marked by a relatively narrow, straight and steep north-dipping fault zone, the Machaoying fault zone, which is a normal fault associated with the Cenozoic rift basin to the north. The southern border of the South Qinling, separating it from the South China block, is the Mianlue suture, which was greatly modified by Late Mesozoic thrusting. The detailed geological framework and tectonic evolution of the Qinling region have been described by Xue et al. (1996), Meng and Zhang (2000), and Ratschbacher et al. (2003). The belt of Mo mineralization spans both the southern margin of the North China block and North Qinling.

The southern margin of the North China block is composed of the Archaean (2806–2841 Ma; Kröner et al., 1988) Taihua high-grade terrain and Dengfeng granite–greenstone terrain (2512 Ma; Kröner et al., 1988). Most of the Mo deposits occur in the Taihua terrain. The Mesoproterozoic Xionger group (1840 Ma; Sun et al., 1991), consisting of alkaline and bimodal volcanics overlying the Tietonggou quartzite covers most of this terrain over an area of 60,000 km^2. The Meso- to Neoproterozoic Guandaokou and Luanchuan groups are a succession of carbonate, phyllite, sandstone, quartzite, trachyandesite and trachyte. This sequence is topped by the Lower Cambrian continental Luoquan tillite and Cambrian–Ordovician platform carbonates, shale and sandstone typical of the North China block (Gao et al., 1996). Locally, Triassic clastic rocks of alluvial and fluvial facies, Jurassic terrigenous strata and Cretaceous terrigenous volcano-sedimentary (lacustrine) rocks are present (Mao et al., 2008). Cambrian and Lower Ordovician clastic rocks and carbonate rocks are extensively developed, and are part of the sedimentary platform cover succession of the North China block. Two types of Proterozoic metamorphic complexes, covering much of the surface area of the North Qinling, are represented by the Qinling and Kuanping groups. The Paleoproterozoic Qinling group (2172–2226 Ma; Zhang et al., 1994) is a crystalline basement and consists of amphibolite- to greenschist-facies metagraywackes and marbles that contain graphite. The Kuanping group is a transitional basement group consisting of tholeiitic greenschist and amphibolite with a Sm–Nd age of 1142 Ma (Zhang et al., 1994). This group is internally structured by pervasive foliations and recumbent isoclinal folds. These features distinguish the transitional basement from crystalline basement in composition, deformation style and metamorphic grade (Meng and Zhang, 2000). In the North Qinling, Middle-to-Upper Paleozoic successions consist of alluvial and fluvial clastic rocks. The Upper Triassic and Jurassic are missing in most parts of the Qinling orogen, but Cretaceous and Cenozoic red beds are common in fault-bounded basins (Mao et al., 2008).

2.2. Geology of the Huanglogpu deposit and sample provenance

The Huanglongpu Mo deposit occurs in the southernmost margin of the North China block. This region, known as Lesser Qinling, consists of several structural components, the oldest of which is a basement of highly deformed and metamorphosed Archean to Paleoproterozoic rocks (Xue et al., 1996). This basement is overlain by a Mesoproterozoic sedimentary sequence formed in a continental-basin setting and a succeeding Neoproterozoic to Middle Ordovician package deposited in a passive continental-margin setting. The Huanglongpu area is characterized by an extensional structure. The ore bodies extend discontinuously over a total distance of about 6 km and are mainly controlled by a northwest-striking fault zone. The deposit is composed of four ore fields at Yuantou, Dashigou, Shijiawan I, II and Taoyuan. With the exception of Shijiawan I, which is hosted by porphyry, the rest of the deposits are associated with carbonatite dykes.

The carbonatite dykes consist of calcite, quartz, potassium feldspar, barite, pyrite, galena, sphalerite, molybdenite, REE-fluorocarbonates [$Ca_xREE_y(CO_3)_{x+y}F_y$], monazite ($REEPO_4$) and brannerite (UTi_2O_6). Minor fluorite is found at Shijiawan and Taoyuan. Alteration envelopes consisting of biotite, epidote, pyrite and anhydrite are developed only at the selvages of the dykes. This distinguishes the Huanglongpu mineralization from the porphyry-type deposits, where an alteration envelope is typically zoned from an inner K-silicate assemblage outward to a propylitic assemblage, with later sericitic alteration cross-cutting the K-silicate zone or occurring near the potassic–propylitic interface (Seedorff and Einaudi, 2004b; Seedorff et al., 2005; Mao et al., 2008; Rusk et al., 2008). In the carbonatites, molybdenite occurs mainly as disseminated grains and intergranular films (Fig. 2). Disseminated molybdenite is also found along fractures in metasomatized gneiss near its contact with the dykes. In the Shijiawan I orebodies, the disseminated and stockwork molybdenite, pyrite, fluorite, potassium feldspar and strong silicification are observed in a roof pendant composed of porphyry and host basaltic rocks of the Xionger group. The exact ore reserve at Yuantou has not been reported, whereas a surface evaluation of this deposit indicated about 1700 t of Mo at a grade of 0.07–0.144% (Geological Team no. 13, 1989). The Dashigou, Shijiawan I, II and Taoyuan orebodies have current reserves of 8.9×10^4, 8×10^4, 6×10^4 and 3.8×10^4 t of Mo with a grade of 0.075–0.103%, 0.071% (average), 0.041–0.104% and 0.041–0.096% Mo, respectively. The samples examined in the present work were collected from the Yuantou, Dashigou and Shijiawan II ore fields.

3. Analytical methods

The major-element compositions of selected major and accessory mineral phases from the Huanglongpu carbonatites were measured by wavelength-dispersive X-ray spectrometry (WDS) using a Cameca SX 100 electron microprobe at the Joint Electron Microscopy and Microanalysis Laboratory (Institute of Geological Sciences, Masaryk University and Czech Geological Survey). The instrument was operated at a beam current of 10 nA and an accelerating voltage of 15 kV. The beam was defocused to a spot size of 5–10 μm to minimize beam-induced damage and thermal decomposition of such heat-sensitive mineral phases as carbonates and feldspars. The following standards and X-ray emission lines were used in the analysis: dolomite (Mg, Kα),

Fig. 2. Photomicrographs showing characteristic textures of the Huanglongpu carbonatites (backscattered-electron images). Cal, calcite; Py, pyrite; Sp, sphalerite; Gn, galena; Mo, molybdenite; Brt, barite; Mnz, monazite-(Ce); Par, parisite-(Ce); Y–Mg, unknown Y–Mg silicate; Bas, bastnäsite-(Ce).

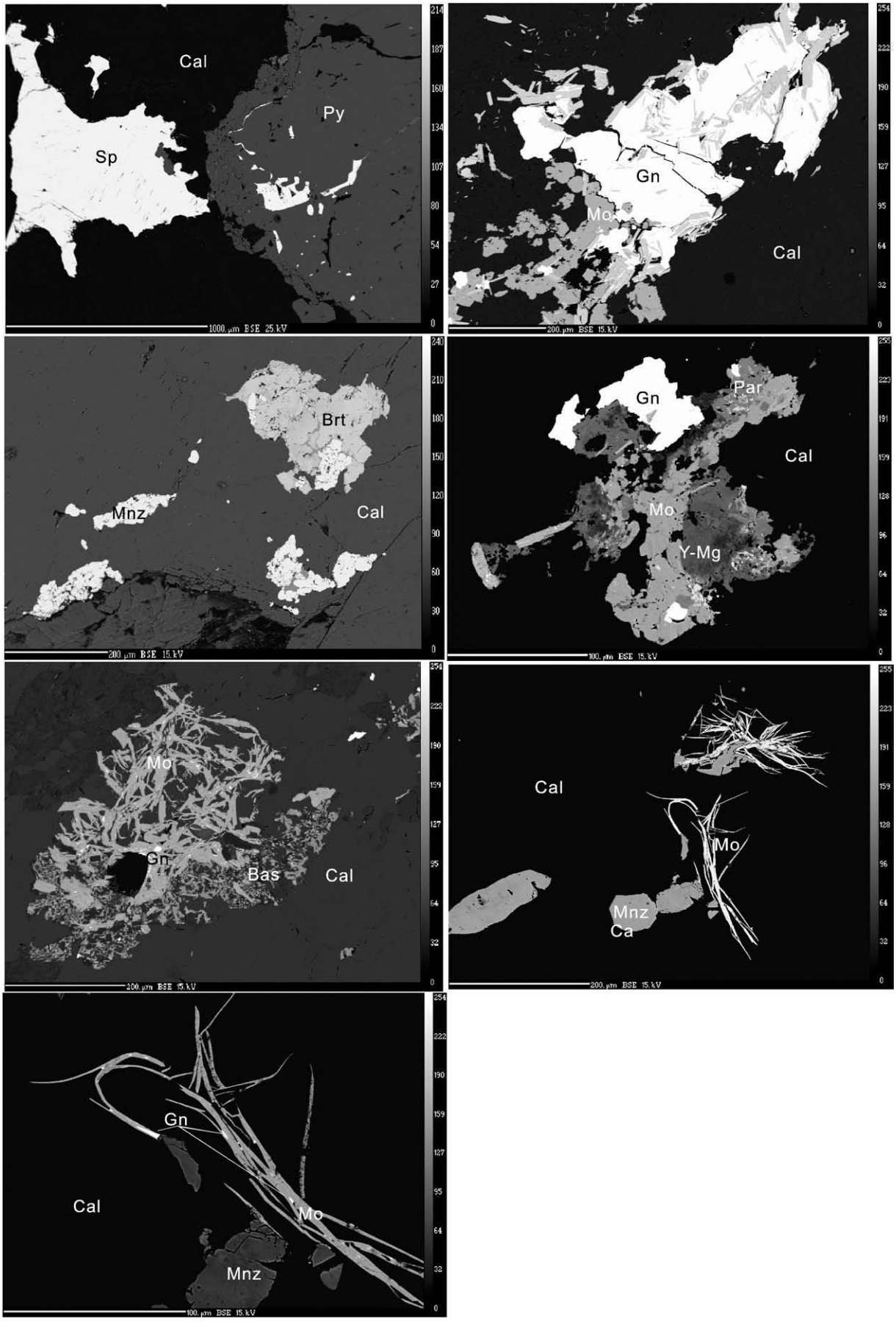
Cal
Py
Sp
1000.μm BSE 25.kV
Gn
Mo
Cal
200.μm BSE 15.kV
Brt
Mnz
Cal
200.μm BSE 15.kV
Gn
Par
Cal
Mo
Y-Mg
100.μm BSE 15.kV
Mo
Gn
Bas
Cal
200.μm BSE 15.kV
Cal
Mo
Mnz
Ca
200.μm BSE 15.kV
Gn
Cal
Mo
Mnz
100.μm BSE 15.kV

Table 1
Representative compositions (wt.%) of calcite and potassium feldspar from the Huanglongpu carbonatites.

Oxide	Calcite				
FeO	0.28	0.32	0.33	0.38	0.26
MnO	2.02	2.19	2.30	2.53	2.25
MgO	0.31	0.26	0.49	0.34	0.24
CaO	52.86	52.96	51.74	53.08	52.76
SrO	0.73	0.67	0.98	1.27	0.63
*CO_2	43.52	43.74	43.18	44.37	43.49
Total	99.72	100.14	99.02	101.97	99.63

*CO_2 was calculated on the basis of stoichiometry.

Oxide	Feldspar		
Na_2O	0.27	0.26	0.17
SiO_2	65.13	64.01	64.83
Al_2O_3	18.24	18.39	18.06
SrO	0.0	0.0	0.05
BaO	0.19	0.56	0.0
K_2O	15.98	16.21	16.49
FeO	0.09	0.10	0.0
Total	99.90	99.53	99.60

Ca and Pb were sought, but not detected.

calcite (Ca, Kα), willemite (Mn, Kα), olivine (Fe, Kα) and celestine (Sr, Lα) for calcite; albite (Na, Kα), sanidine (Al, Si and K, Kα line for all), titanite (Ca, Kα), galena (Pb, Mα), celestine (Sr, Lα), barite (Ba, Lα) and andradite (Fe, Kα) for feldspars; galena (Pb, Mα), sphalerite (Zn, Kα), pyrite (Fe, Kα), pararammelsbergite (Ni and As with Kα and Lb, respectively), chalcopyrite (S, Kα) and pure Cu, Mo, Co, Se, Ag, Re, Sb and Bi (Cu–Ag with Lα; Re and Sb with Lb; Bi with Mb) for sulfides; andradite (Ca and Fe, Kα for both), sanidine (Al and K, both with Kα), titanite (Si, Kα), celestine (Sr, Lα), barite (S and Ba with Kα and Lα, respectively) and galena (Pb, Mα) for sulfates. For the analysis of minerals containing rare-earth elements (REE), andradite (Si, Kα), wollastonite (Ca, Kα), apatite (P, Kα), barite (S, Kα), celestine (Sr, Lα), topaz (F, Kα), synthetic ThO_2 (Th, Mα) and U (U, Mb), synthetic Y–Al garnet (Y, Kα), REE glasses and orthophosphates (La, Ce and Sm with Lα lines; Pr, Nd, Gd and Dy with Lβ lines) were used. The data were reduced and corrected using the PAP routine (Pouchou and Pichoir, 1984).

The abundances of trace elements (including REE) in fresh carbonatite samples were determined by inductively-coupled–plasma mass-spectrometry (ICP–MS) at the Institute of Geochemistry of the Chinese Academy of Sciences. Prior to the analysis, 50 mg of rock powder were dissolved in a Teflon bomb using 1 ml of HF (38%) and 0.5 ml of HNO_3 (68%). The sealed bomb was placed in an electric oven and heated to 190 °C for 24 h. The cooling solution was spiked with 1 ml of 1 μg ml^{-1} Rh, used as an internal standard, and evaporated on a hot plate. This was followed by 2 cycles of dilution with 1 ml of HNO_3 and evaporation to dryness. The final residue was re-dissolved in 8 ml of HNO_3. The bomb was re-sealed, returned to the oven and heated to 110 °C for 3 h. The final solution was diluted to 100 ml by addition of distilled de-ionized water for ICP–MS analysis. The analytical precision for most elements is generally better than 10%. Further details of this analysis are given in Liang et al. (2000).

Table 3
Representative compositions (wt.%) of sulfate minerals from the Huanglongpu carbonatites.

Oxide	Barite-celestine series				
CaO	1.18	0.09	0.34	0.07	1.26
SiO_2	0.0	0.0	0.07	0.0	0.0
K_2O	0.06	0.0	0.0	0.0	0.0
Na_2O	0.08	0.12	0.10	0.12	0.10
Al_2O_3	0.20	0.42	0.30	0.33	0.21
SrO	28.79	1.29	12.65	0.48	26.75
BaO	31.05	64.46	50.50	63.21	33.45
SO_3	39.63	33.62	35.58	33.59	38.41
Total	100.99	100.0	99.54	97.80	100.18

Fe and Pb were sought, but not detected in any of the samples.

The carbon and oxygen isotopic compositions of calcite were measured in the Institute of Geochemistry, Chinese Academy of Sciences, using an Iso-Prime continuous-flow isotope-ratio mass spectrometer. The results are expressed in the conventional δ-notation, i.e. $\delta = (R_1/R_2 - 1) \times 1000$, where R_1 is the $^{13}C/^{12}C$ or $^{18}O/^{16}O$ ratio in the sample and R_2 is the corresponding isotope-ratio in the standard (V-PDB for C and V-SMOW for O), expressed in per mil (‰). Analytical reproducibility is ±0.1‰ for both C and O.

4. Results

4.1. Mineral chemistry

The representative major-element compositions of carbonates, feldspars, sulfides, sulfates and REE minerals are given in Tables 1–4. Calcite is the principal rock-forming carbonate mineral in the Huanglongpu carbonatites. It contains high Sr and Mn contents (0.6–1.3 and 2.0–2.5 wt.% respective oxides), but low levels of Mg and Fe (0.2–0.5 and 0.3–0.4 wt.% respective oxides; Table 1). Euhedral phenocrysts of alkali feldspar are a modally significant constituent of the carbonatites (up to 5%). They consist of orthoclase showing the compositional range $Or_{81-97}Ab_{2-18}An_{0-0.1}$ (mineral symbols after Kretz, 1983). The mineral has low Sr and Ba abundances (<0.05 and 0.6 wt.% respective oxides; Table 1), which are much lower than in primary potassium feldspar from other carbonatites (up to 0.5 and 7.4 wt.%, respectively; Reguir and Mitchell, 2000; Reguir, 2001; Chakhmouradian et al., 2008). The low Sr and Ba contents indicate that the feldspar in the Huanglongpu rocks may be of deuteric origin rather than having crystallized from carbonatitic magma.

Sulfides are the most common minor and accessory constituents of the carbonatites. The dominant sulfide phases are coarse-grained pyrite, followed by galena, sphalerite and molybdenite. These phases

Table 2
Representative compositions (wt.%) of sulfide minerals from the Huanglongpu carbonatites.

Element	Pyrite		Galena				Sphalerite		Molybdenite				
Pb	0.05	0.10	85.72	85.13	85.55	87.11	0.24	0.08	0.0	0.0	0.0	0.0	0.70
Zn	0.0	0.0	0.0	0.0	0.0	0.06	65.70	65.80	0.0	0.0	0.0	0.0	0.0
Fe	46.77	46.65	0.0	0.0	0.0	0.0	0.42	0.51	0.0	0.0	0.0	0.08	0.26
Cu	0.0	0.0	0.0	0.0	0.0	0.0	0.06	0.09	0.0	0.0	0.0	0.0	0.0
Mo	0.0	0.0	0.0	0.0	0.0	0.0	1.18	1.30	60.24	60.47	60.37	60.71	59.67
Re	0.0	0.0	0.15	0.24	0.23	0.22	0.0	0.0	0.42	0.32	0.38	0.22	0.27
Bi	0.0	0.0	0.63	0.81	0.63	0.35	0.0	0.0	0.0	0.0	0.0	0.0	0.0
Ag	0.0	0.07	0.09	0.12	0.0	0.0	0.09	0.0	0.11	0.0	0.0	0.0	0.05
S	52.14	52.05	13.68	13.66	13.65	13.39	31.0	30.50	39.41	39.39	39.52	39.58	38.91
Total	98.96	98.87	100.27	99.96	100.06	101.13	98.69	98.28	100.18	100.18	100.27	100.59	99.86

The Co, Ni, As, Se and Sb contents of sulfides are close or below the detection limits of WDS.

Table 4
Representative compositions (wt.%) of REE minerals from the Huanglongpu carbonatites.

Oxide/element	Parisite-(Ce)				Bastnäsite-(Ce)						Monazite-(Ce)					
CaO	11.06	10.87	10.46	10.72	9.89	10.24	0.18	0.31	0.26	0.42	0.12	0.20	0.09	0.19	0.65	0.37
P_2O_5	0.0	0.0	0.0	0.0	0.0	0.0	0.0	0.0	0.0	0.0	0.0	29.11	28.95	29.32	29.95	29.60
SrO	0.12	0.16	0.45	0.14	0.0	0.68	0.0	0.0	0.0	0.0	0.0	0.0	0.07	0.15	0.0	0.0
SiO_2	0.08	0.13	0.24	0.0	0.34	0.18	0.09	0.13	0.18	0.19	0.06	0.46	0.50	0.42	0.65	0.61
SO_3	0.0	0.0	0.0	0.0	0.0	0.0	0.0	0.0	0.0	0.0	0.0	0.0	0.15	0.24	0.44	0.79
ThO_2	0.0	0.06	0.14	0.0	0.05	0.0	0.15	0.09	0.11	0.13	0.0	1.14	0.95	1.18	0.78	0.05
Y_2O_3	1.19	1.39	1.79	0.75	1.22	0.33	0.44	0.36	0.40	0.33	0.32	0.57	0.36	0.48	0.06	0.07
La_2O_3	14.92	10.04	11.89	13.02	14.66	14.07	16.73	21.24	20.55	20.39	20.83	18.72	19.67	20.74	19.99	22.70
Ce_2O_3	24.83	26.16	25.47	25.64	26.28	25.11	38.45	36.18	35.39	35.11	35.72	33.03	33.28	33.06	34.45	33.35
Pr_2O_3	3.01	3.53	3.59	3.46	3.53	3.30	3.91	3.35	3.56	3.72	3.44	3.04	2.95	2.75	2.82	2.44
Nd_2O_3	10.61	12.59	11.26	12.33	11.32	12.61	13.46	11.70	12.36	12.17	12.75	9.70	9.02	8.13	8.34	7.64
Sm_2O_3	2.09	2.65	2.49	1.82	1.68	1.70	1.62	1.45	1.33	1.58	1.74	1.28	1.18	0.91	0.80	0.82
Gd_2O_3	1.39	1.83	1.28	1.06	0.78	0.72	0.43	0.46	0.38	0.54	0.58	0.58	0.43	0.32	0.07	0.22
Dy_2O_3	0.42	0.67	0.58	0.31	0.32	0.23	0.17	0.11	0.13	0.11	0.21	0.21	0.14	0.13	0.0	0.0
F	5.93	5.30	6.70	5.48	5.71	6.67	7.93	7.81	6.46	7.52	7.76	0.67	0.66	0.72	0.69	0.70
CO_2*	2.20	2.50	1.81	2.34	2.23	1.74	0.41	0.47	1.07	0.59	0.49					
H_2O*	24.48	24.49	24.34	24.12	24.11	23.96	20.37	20.40	20.21	20.29	20.37					
F=O	−2.50	−2.23	−2.82	−2.31	−2.40	−2.81	−3.34	−3.29	−2.72	−3.17	−3.27	−0.28	−0.28	−0.30	−0.29	−0.29
Total	99.83	100.14	99.67	98.88	99.72	98.73	101.0	100.77	99.67	99.92	101.12	98.43	98.12	98.44	99.40	99.07

* CO_2 and H_2O compositions are calculated by charge balance. U was sought, but not detected in any of the samples.

generally form euhedral to subhedral crystals and occur as two distinct assemblages: (1) pyrite + sphalerite + trace amounts of galena; (2) galena + molybdenite ± REE-bearing minerals (Fig. 2). The Cu, Co, Ni, As, Se, Sb and Ag contents in the sulfides are low (in most cases, at or below the detection limits of WDS; Table 2). Galena contains appreciable Bi (0.3–0.8 wt.%), which was not detected in any of the other sulfides. The Re content ranges from below the limits of detection in pyrite and sphalerite to 0.1–0.2 wt.% in galena and up to 0.4 wt.% in molybdenite.

Sulfates of white, pale green and yellowish color are common accessory minerals. Compositionally, they correspond to intermediate members of the celestine-barite series with generally low levels of Ca (<1.3 wt.%) and other substituent elements. Most compositions range between $Brt_{99}Cls_1$ and $Brt_{42}Cls_{54}Anh_4$ (mineral symbols after Kretz, 1983; Table 3).

REE minerals, including REE-fluorocarbonates and monazite-(Ce), are characteristic accessory constituents of the examined carbonatites (Table 4). The REE-fluorocarbonates occur as (1) discrete pseudomorphs after an unidentified Y–Mg silicate, and (2) in intimate intergrowths with molybdenite and/or galena (Fig. 2). The two major fluorocarbonates identified in the Huanglongpu samples are bastnäsite-(Ce) and parisite-(Ce) [$REE(CO_3)F$ and $CaREE(CO_3)_2F$, respectively]. The two minerals exhibit notably different chondrite-normalized REE patterns (Fig. 3); parisite-(Ce) has lower levels of La and Ce, but is enriched in mid- and heavy REE relative to bastnäsite-(Ce). The $(La/Nd)_n$ ratio averages 2.1 in parisite-(Ce) and 3.1 in bastnäsite-(Ce). In common with the REE-fluorocarbonates, the Huanglongpu monazite-(Ce) is strongly enriched in light REE (LREE) (Fig. 3); its $(La/Y)_n$ values overlap the $(La/Y)_n$ range of bastnäsite-(Ce) (on average, 1142, 399, respectively), but are much higher than in parisite-(Ce) (average 119). The $(La/Nd)_n$ ratio of monazite-(Ce) (on average, 4.6) is higher than that of the REE-fluorocarbonates. Also in contrast to the REE-fluorocarbonates, the monazite-(Ce) hosts appreciable amounts of Th and, to a lesser extent, S (up to 1.2 wt.% ThO_2 and 0.8 wt.% SO_3). The elevated Th contents coupled with low to undetectable U are typical of monazite from carbonatites and related igneous rocks (Chakhmouradian and Mitchell, 1998, 1999; Smith et al., 2000; Le Bas et al., 2004; Wall and Zaitsev, 2004; Wall et al., 2008).

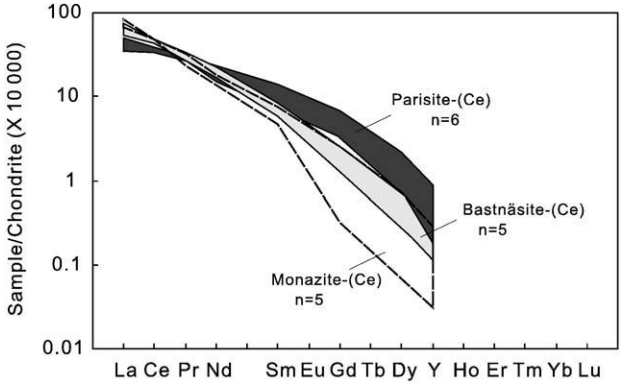

Fig. 3. Chondrite-normalized REE abundances in the major REE minerals from the Huanglongpu carbonatites. Normalization values are from McDonough and Sun (1995).

4.2. Whole-rock geochemistry

The bulk carbonatite samples from the three ore fields show broadly similar trace-element compositions, except for the abundances of U, Nb and Mo, which reflect variations in the distribution of Nb-bearing brannerite and molybdenite (Table 5). The carbonatites are strongly enriched in large-ion lithophile elements (LILE), particularly Sr, Ba and Pb, REE and U, but not in high-field-strength elements (HFSE = Zr, Hf, Nb and Ta) relative to the primitive mantle (Fig. 4). Mantle-normalized patterns for selected trace elements (except for the Yuantou samples) show anomalously high Ba, U, Pb and Mo abundances relative to the neighboring incompatible elements. In comparison with the "average carbonatite" (Chakhmouradian et al., 2008), the Huanglongpu samples are depleted in Th and HFSE. In these samples, the Nb/Ta (average 4.4, 31, 10.3 for Yuantou, Dashigou and Shijiawan, respectively) and Zr/Hf (average 0.3, 0.3, 0.1 for Yuantou, Dashigou and Shijiawan, respectively) ratios are significantly lower than the "average carbonatite" values of 35 and 60 (Chakhmouradian, 2006). However, the Mo contents of the Dashigou and Shijiawan rocks are generally higher than the average calciocarbonatite value of 12 ppm (Chakhmouradian, unpubl. data). Another unusual geochemical feature of the Huanglongpu carbonatites is their enrichment in heavy REE (HREE) and Y (370–1130 ppm Y + Gd…Lu), unparalleled by most other carbonatites worldwide except in some Namibian localities and Huayangchuan, China (e.g., Eby, 1975; Nelson et al., 1988; Woolley and Kempe, 1989; Xu et al., 2007; Wall et al., 2008, and references therein). The chondrite-normalized REE patterns are essentially flat and show only slight LREE enrichment with an average $(La/Yb)_n$ value of 1.4, 2.7, 1.2 for Yuantou, Dashigou and Shijiawan, respectively (Fig. 5).

Table 5
Trace-element composition (ppm) of carbonatites from Yuantou (YT), Dashigou (DSG) and Shijiawan (SJW) ore fields.

Samples	YT-1	YT-2	DSG-1	DSG-2	DSG-3	DSG-4	DSG-5	DSG-6	DSG-7	DSG-8	DSG-9	DSG-10	DSG-11	DSG-12	SJW-1	SJW-2	SJW-3
Rb	0.53	0.21	0.19	0.32	0.215	0.158	4.17	2.20	0.52	0.81	0.25	0.35	0.71	0.31	1.02	0.67	2.10
Ba	478	758	354	656	537	916	145	325	188	542	308	397	379	529	274	563	225
Th	0.54	0.17	0.22	0.83	0.06	1.47	1.35	0.25	0.57	1.51	0.40	0.14	1.00	3.76	0.27	1.58	0.22
U	0.49	0.22	1.59	21.9	0.36	0.76	4.67	0.83	1.22	10.4	0.23	0.24	1.58	0.50	1.14	4.62	1.64
Nb	1.19	0.24	1.02	24.0	0.14	0.34	2.59	5.09	0.94	6.16	0.26	0.31	0.77	0.21	0.67	2.37	1.30
Ta	0.18	0.14	0.27	0.12	0.08	0.14	0.12	0.08	0.17	0.10	0.12	0.49	0.11	0.11	0.15	0.09	0.18
Pb	105	85.0	68.8	72.0	63.1	133	302	138	74.9	396	105	347	153	68.3	82.5	69.3	86.0
Mo	0.63	0.94	33.8	610	0.79	51.0	240	20.9	11.0	1 010	8.29	19.2	2.63	32.6	39.6	38.5	86.3
Sr	6595	5900	5840	5570	6430	4740	2290	4603	6010	4470	5240	5078	5 640	5880	5390	4506	5186
Zr	0.33	0.08	0.12	0.19	0.14	0.17	0.34	0.18	0.18	0.36	0.08	0.18	0.27	0.21	0.13	0.12	0.12
Hf	0.65	1.01	0.90	0.58	0.42	0.89	0.79	0.56	1.04	0.55	0.88	1.21	0.79	0.78	0.97	0.51	1.28
Y	725	560	575	376	192	497	429	284	571	274	569	559	367	367	721	417	712
La	166	126	124	144	167	420	211	145	373	147	181	106	377	457	128	233	106
Ce	967	343	349	338	467	993	467	302	923	348	427	248	873	1000	310	485	256
Pr	58.0	55.7	56.8	48.7	60.6	136	63.8	39.8	116	47.5	57.3	35.6	108	118	43.2	60.7	36.4
Nd	272	263	261	210	247	586	264	177	497	202	265	170	456	471	199	260	169
Sm	76.0	80.7	75.0	53.2	48.6	129	64.4	41.1	94.2	44.3	70.2	52.6	84.2	82.9	58.8	57.5	51.5
Eu	0.33	0.08	21.7	15.0	12.9	33.1	18.2	11.7	23.9	12.5	21.0	16.6	21.6	21.3	18.2	16.3	16.6
Gd	0.65	1.01	80.7	59.0	49.4	120	69.9	45.4	100	47.8	80.3	69.6	83.6	85.2	71.6	58.7	71.9
Tb	22.3	23.9	13.8	9.70	7.05	16.0	11.2	6.76	14.0	7.23	13.3	11.6	11.3	11.1	12.6	9.00	12.0
Dy	84.5	88.7	82.5	56.8	39.3	82.6	65.6	41.9	81.3	43.5	86.1	78.6	60.6	60.6	90.2	58.3	86.6
Ho	20.2	21.4	20.1	13.9	9.65	18.5	15.8	10.1	21.0	11.4	19.9	19.0	15.0	14.9	23.1	14.0	22.4
Er	60.6	62.6	62.4	43.1	30.4	56.4	48.4	32.8	70.3	39.3	62.4	60.3	48.6	49.1	76.8	45.4	75.8
Tm	10.2	9.73	10.1	6.94	4.51	8.70	7.78	5.66	11.6	6.76	10.4	10.4	7.83	8.01	13.7	7.92	13.7
Yb	67.4	68.4	74.8	51.1	31.1	63.4	57.0	42.7	86.5	54.0	76.0	78.0	59.1	60.7	105	59.7	105
Lu	10.1	9.54	11.0	7.70	4.35	9.32	8.29	6.74	12.6	8.90	11.8	11.7	9.32	9.33	16.1	9.10	16.0

4.3. Stable-isotope compositions

The C and O isotopic data for rock-forming calcite from the Yuantou and Dashigou carbonatites are summarized in Table 6. The most striking feature of the analyzed samples is their remarkably uniform isotopic compositions with average $\delta^{13}C$ values of −6.6‰ and −6.7‰, and $\delta^{18}O$ values of 9.2‰ and 7.9‰ for the Yuantou and Dashigou samples, respectively. These data are similar to those for the earlier-described Shijiawan carbonatites (on average, −6.8‰ $\delta^{13}C$ and 9.1‰ $\delta^{18}O$: Xu et al., 2007). These compositions are consistent with a primary mantle-derived signature unaffected by surface alteration or hydrothermal overprint (Fig. 6).

5. Discussion

5.1. Molybdenite mineralization in carbonatites

The available geochemical evidence leaves no doubt that the Huanglongpu carbonatites are igneous rocks of mantle provenance. They are characterized by high Sr and REE contents (Fig. 4), similar to other carbonatites elsewhere in the world (Eby, 1975; Nelson et al., 1988; Woolley and Kempe, 1989; Hornig-Kjarsgaard, 1998; Chakhmouradian et al., 2008; and references therein). The rock-forming calcite shows high Sr and Mn abundances (Table 1) characteristic of carbonatites, but uncommon in sedimentary carbonates. The latter typically contain low levels of Sr and Mn not exceeding 100 ppm (Tucker and Wright, 1990; Veizer et al., 1992). Yang and Le Bas (2004) suggested that the Sr and Mn contents of carbonate minerals can be used to discriminate igneous rocks from metamorphosed sedimentary carbonates. In addition, the Huanglongpu samples show $\delta^{13}C_{PDB}$ and $\delta^{18}O_{SMOW}$ values indicative of a primary mantle, rather than crustal, source (Fig. 6).

With the exception of the Shijiawan I orebody, the molybdenite mineralization at Huanglongpu is spatially associated with carbonatite dykes (Fig. 1). Molybdenite from the Dashigou deposit gave a Re–Os age of 221 Ma (Huang et al., 1995; Stein et al., 1997), which is significantly older than the age of the spatially close Shijiawan granite porphyry complex (124 Ma: Huang et al., 1995) and its associated Mo mineralization (138–140 Ma: Mao et al., 2008). Therefore, the molybdenite mineralization examined in the present work can be

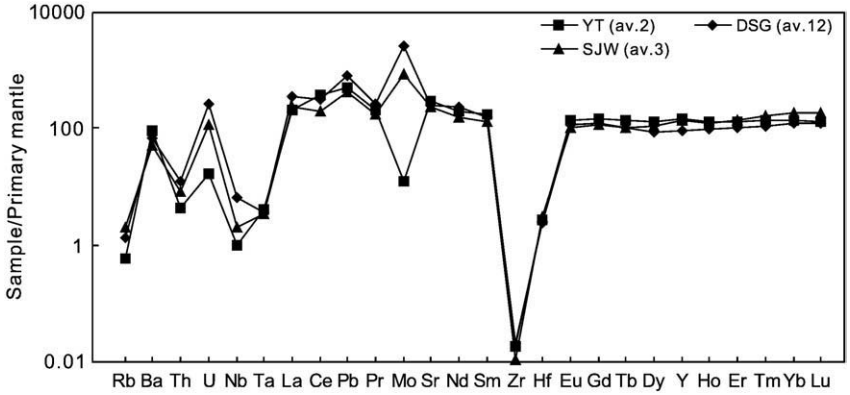

Fig. 4. Primitive mantle-normalized trace-element abundances in whole-rock samples of carbonatites from the Yuantou (YT), Dashigou (DSG) and Shijiawan II (SJW) ore fields. Normalization values are from McDonough and Sun (1995).

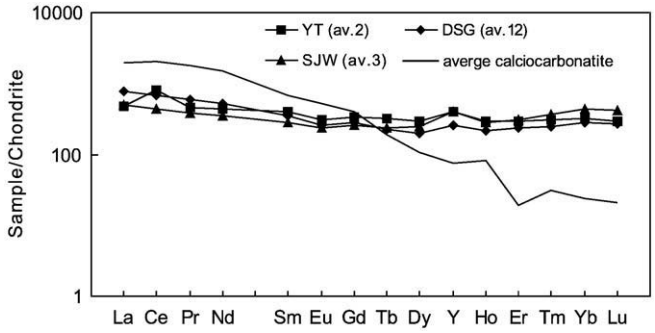

Fig. 5. Chondrite-normalized REE abundances in whole-rock samples of carbonatites from the Yuantou (YT), Dashigou (DSG) and Shijiawan II (SJW) ore fields in comparison to average calciocarbonatite (Woolley and Kempe, 1989).

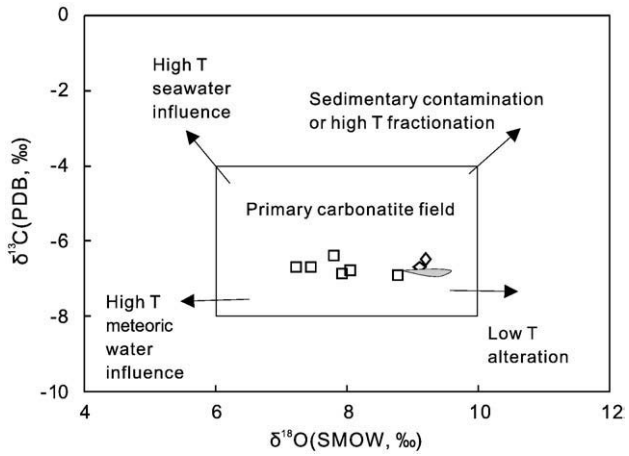

Fig. 6. Carbon and oxygen isotopic compositions of calcite from the carbonatites of Dashigou (squares), Yuantou (diamonds) and Shijiawan II (shaded field, after Xu et al., 2007). Shown for comparison are the field of primary, unmodified carbonatites (after Keller and Hoefs, 1995) and the major processes responsible for changes in C–O isotopic composition of carbonatites (Demény et al., 1998).

considered cogenetic with its host LILE-enriched carbonatites. The uniform stable-isotopic composition of calcite from the carbonatites, absence of ^{18}O-rich carbonates and consistently low $\delta^{18}O_{SMOW}$ values of quartz from the Yuantou and Dashigou orebodies (8.8–9.8 and 8.1–10.2‰, respectively: Xu et al., unpubl. data) all indicate that the ore-forming fluids were of magmatic origin and were not contaminated through interaction with groundwater, meteoric water, or fluids derived from the crustal wall-rocks.

To date, molybdenite formation has been studied mostly in relation to porphyry-type deposits. Landtwing et al. (2005) have recognized several processes triggering precipitation of sulfides from magmatic–hydrothermal fluids, including rapid changes in pressure (P) and/or temperature (T), fluid phase separation into coexisting a high-salinity brine and low-salinity vapor, fluid–rock interaction, and dilution of magmatic brines by meteoric water. Importantly, most of the published studies are focused on porphyry Cu–Mo systems, but do not even acknowledge that Mo and Cu differ significantly in their geochemical characteristics. For example, Rusk et al. (2004) found that fluid inclusions in molybdenite-bearing quartz veins contain less than detectable concentrations of Mo even though their Cu content is high. The distribution of Re in molybdenite from 75 porphyry Cu–Mo and Mo–Cu deposits shows that molybdenite in porphyry Mo and Mo–Cu deposits contains significantly lower Re abundances than that in porphyry Cu and Cu–Mo deposits (Berzina et al., 2005). Experimental studies indicate that Cl and S complexes are the principal forms of Cu transport in fluids (Simon et al., 2006), whereas Mo can be transported as either Cl-species or H_2MoO_4 even at very low concentrations of chlorine in the fluid (Ulrich and Mavrogenes, 2008). In addition, the mechanisms of Mo and Cu precipitation in hydrothermal systems are probably different. Rusk and Reed (2002), Rusk et al. (2008) suggested that precipitation of molybdenite is triggered by a drop in P from near-lithostatic to near-hydrostatic conditions, whereas precipitation of Cu phases associated with Pb, Zn, Ag and As mineralization likely involves a decrease in T that may not be accompanied by any changes in P. This interpretation is consistent with the conclusions of Landtwing et al. (2005).

The Climax-type Mo deposits represent an “end-member” of porphyry-hosted mineralization characterized by high Mo abundances, but very low concentrations of Cu. Klemm et al. (2008) suggested that fluid phase separation by decompression from near-lithostatic to near-hydrostatic conditions led to the removal of a large amount of Cu-enriched vapor accompanied by extreme Mo enrichment in the residual Cu–S-poor brine that eventually produced such Mo-dominant porphyry systems. The contrasting partitioning of Mo and Cu between the consanguineous brine and vapor results in spatial variations in Cu/Mo ratio, manifested as zoning within porphyry deposits, or late-stage base-metal mineralization cross-cutting quartz–molybdenite veins (e.g., Seedorff and Einaudi, 2004b; Audétat et al., 2008; Rusk et al., 2008). However, the vapor–brine immiscibility model cannot explain formation of molybdenite in carbonatitic systems. The Huanglongpu orebodies lack any evidence of zoned distribution of Mo and Cu. Copper sulfides are characteristically absent, whereas the Cu content of sulfide minerals is very low to undetectable. Instead, the Huanglongpu molybdenite is invariably associated with REE minerals and galena (Fig. 2), which likely indicates genetic linkage between these minerals. Carbonatites are known to contain the highest amounts of LREE among all igneous rocks, and these elements may be incorporated in both early cumulus phases and late-stage deuteric phases (Woolley and Kempe, 1989; Hornig-Kjarsgaard, 1998; Wall and Zaitsev, 2004; Xu et al., 2008). Bühn and Rankin (1999) analyzed the composition of alkali-(H_2O,CO_2, Cl,F)-rich carbonatite-derived fluids trapped under closed-system conditions and concluded that REE, Cu, Pb, Sr, Ba and other LILE partition into the fluid relative to the parental magma. When released from their host, REE-enriched fluids produce an overprinted secondary mineralization (Costanzo et al., 2006). Xu et al. (2008) suggested that REE are strongly enriched in volatile-rich fluids expelled from carbonatitic magma owing to very low partition coefficients of these elements in rock-forming carbonates relative to a melt. This enrichment may ultimately produce REE mineralization of economic-scale. At Huanglongpu, the available petrographic and geochemical evidence indicates that cumulate precipitation of calcite was an important component of the differentiation of carbonatitic magma (Xu et al., 2007). Therefore, it is feasible that, in common with REE, Mo (and probably Pb) fractionated into a volatile-rich carbonatitic fluid in the course of magma evolution.

Table 6
C–O isotopic compositions of calcites from Yuantou (YT) and Dashigou (DSG) carbonatites.

Sample	YT-1	YT-2	DSG-1	DSG-2	DSG-3	DSG-9	DSG-10	DSG-11
$\delta^{13}C_{PDB}$ (‰)	−6.67	−6.49	−6.90	−6.36	−6.85	−6.76	−6.69	−6.67
$\delta^{18}O_{SMOW}$ (‰)	9.13	9.19	8.78	7.81	7.91	8.05	7.22	7.44

5.2. Molybdenum sources

Carbonatites are typically poor in Mo; most of the published compositions are at or just above the lower limit of detection (Woolley and Kempe, 1989). Molybdenite has not been reported from fluid inclusions in minerals from carbonatites (Bühn and Rankin, 1999; Williams-Jones and Palmer, 2002; Costanzo et al., 2006). To our knowledge, the Mo abundances significantly exceeding the "average carbonatite" value of 12 ppm have been reported only from the Salpeterkop complex in South Africa (up to 87 ppm: Verwoerd et al., 1995) and Arshan in eastern Siberia (up to 56 ppm: Doroshkevich et al., 2008). In neither of these cases, however, does the level of Mo enrichment approach economic levels, nor has the source or host of Mo in the carbonatite been identified.

The absence of any structural or temporal connection between the bulk of Mo mineralization and granitic magmatism at Huanglongpu, and the intimate paragenetic association between molybdenite and REE minerals (see above), implies that the observed Mo enrichment is a primary carbonatitic feature. Further, the Huanglongpu rocks are characterized by very high HREE contents uncommon among carbonatites (e.g., Eby, 1975; Woolley and Kempe, 1989; Hornig-Kjarsgaard, 1998; Chakhmouradian et al., 2008 and references therein). The HREE enrichment cannot be attributed to a secondary process (such as reaction of the carbonatite with an invading hydrothermal fluid) because any evidence of such a process is lacking from the C–O isotopic record (Fig. 6). The magma evolution model proposed for the Qinling carbonatites by Xu et al. (2007) also cannot account for the extremely low $(La/Yb)_n$ values (<3) of these carbonatites, indicating that, similar to Mo, the observed enrichment in HREE is a primary feature reflecting the unusual geochemical character of the source of the Huanglongpu carbonatites.

Mao et al. (1999) proposed that, because of the very similar geochemical behavior of Mo and Re, the Re content of molybdenite ultimately depends on the nature of the Mo source. According to these authors, the Re content of molybdenite precipitated from mantle-derived melts/fluids is high (>100 ppm) relative to molybdenite derived from mixed mantle–crustal sources (10–100 ppm) and, especially, that from crustal sources (<10 ppm). This is in accord with the findings of Stein et al. (2001) that deposits genetically linked to mantle underplating and mantle metasomatism, or re-melting of mafic and ultramafic rocks feature significantly higher levels of Re enrichment in molybdenite relative to crustally derived deposits. It is worthy of note here that the Re content of the Huanglongpu molybdenite is much higher than at any other deposit in the Qinling area, i.e. 700–4200 ppm and <180 ppm Re, respectively (Huang et al., 1995; Mao et al., 1999; Li et al., 2007; Mao et al., 2008; this work). The average Re/Mo and Re/Pb values of the associated molybdenite and galena (0.005 and 0.002, respectively) are close to the primitive-mantle values (0.006 and 0.002, respectively; McDonough and Sun, 1995). Thus, the Re budget and the restricted C–O isotopic range of the Huanglongpu carbonatite both indicate that its parental magma did not undergo any significant degassing during its emplacement (Sun et al., 2003; Demény et al., 2004).

The relative importance of source enrichment versus magma/fluid evolution for the generation of economic-level Mo concentrations has been discussed extensively in the literature (e.g., Lehmann, 1988; Stein and Hannah, 1988; Misra, 1999; Klemm et al., 2008). As early as in 1981, Westra and Keith (1981) proposed that Mo in porphyry and related deposits is ultimately derived from the mantle. More recently, Berzina and Borisenko (2008) suggested that long-term interaction of mantle plumes with the lithosphere is essential to the formation of Cu–Mo porphyry systems. In contrast, Lehmann (1987) concluded that, at least in the case of the Climax-type deposits, evidence for anomalous enrichment of the mantle or lower crust in Mo is lacking. The lower crust in the North Qinling segment, as well as the basement of the Taihua, Xionger and Luanchuan Groups in the southern margin of the North China block, which hosts the carbonatites studied in the present work (see Section 2), are estimated to have significantly higher Mo contents (2.04 ppm in the North Qinling and 1.5–15.7 ppm in the North China block) than other major tectonic units in eastern China (Hu et al., 1988; Gao et al., 1998) and the estimated average crustal value (0.6 ppm, Wedepohl, 1995). This regional Mo geochemical anomaly strongly suggests that the source of Mo mineralization at Qinling lies in the lithospheric mantle (Huanglongpu carbonatites) and deep crust modified by mantle-derived fluids (porphyry-type deposits). Although the unique carbonatite-hosted molybdenite deposits of the Huanglongpu area offer convincing evidence that enrichment of the mantle source in Mo is an important impetus (although not a prerequisite: Lehmann, 1988) for the formation of economic-scale mineralization, neither the source nor the process(es) responsible for the enrichment of the Qinling lithosphere in Mo has been established unambiguously. Interaction with a mantle plume (Berzina and Borisenko, 2008) can be ruled out on the basis of geochemical evidence (Xu et al., 2007) and the absence of contemporaneous basaltic and silica–undersaturated alkaline magmatism typically associated with hot spots. A more plausible cause of lithospheric enrichment in Mo is a fluid overprint related to the subduction of Paleo-Tethys beneath the North China block in the Late Permian, i.e. shortly prior to the regional-scale extension in the Late Triassic (Hacker et al., 2004) and emplacement of the Huanglongpu carbonatites (Stein et al., 1997).

6. Conclusions

The geochemical evidence obtained in the present work clearly indicates that carbonatites at Huanglongpu are mantle-derived igneous rocks not affected by secondary processes. The carbonatites contain economic concentrations of molybdenite, which does not show any spatial or temporal connection to the Late Jurassic–Early Cretaceous Mo porphyry deposits in the Qinling area. In contrast to the latter, the Huanglongpu molybdenite contains high levels of Re (0.1–0.4 wt.%), is associated with REE-fluorocarbonates, monazite-(Ce) and Re-bearing galena, and is of much older (Late Triassic) age. These differences indicate that the molybdenite mineralization at Huanglongpu is genetically related to the carbonatites, whose parental magma was inherently rich in Mo. This enrichment was amplified by fractionation of the carbonatitic magmas that produced cumulate calcite with essentially flat REE patterns (Xu et al., 2007) and a fluid strongly enriched in LREE, Mo, Pb and S. The Huanglongpu carbonatites contain some of the highest HREE and Mo contents of all known carbonatites, which implies a geochemically unusual mantle source. Further isotopic and trace-element studies of these rocks are required to ascertain the nature of that source.

Acknowledgments

We thank A.N. Mariano and an anonymous reviewer for reviewing and improving the manuscript. Editorial comments by Nelson Eby also improved sections of this manuscript. We also thank Y.J. Chen for discussion. This research was financially supported by the Chinese National Science Foundation (nos. 40973040 and 40773021) and the Chinese "973" Project (no. 2006CB403508). ARC acknowledges the Natural Sciences and Engineering Research Council of Canada and The Anchor House for their continuing support.

References

Audétat, A., Pettke, T., Heinrich, C.A., Bodnar, R.J., 2008. The composition of magmatic–hydrothermal fluids in barren and mineralized intrusions. Economic Geology 103, 877–908.

Berzina, A.P., Borisenko, A.S., 2008. Porphyry Cu–Mo mineralization and mantle plumes. Doklady Earth Sciences 423, 1240–1244.

Berzina, A.N., Sotnikov, V.I., Economou-Eliopoulos, M., Eliopoulos, D.G., 2005. Distribution of rhenium in molybdenite from porphyry Cu–Mo and Mo–Cu deposits of Russia (Siberia) and Mongolia. Ore Geology Reviews 26, 91–113.
Bühn, B., Rankin, A.H., 1999. Composition of natural, volatile-rich Na–Ca–REE–Sr carbonatitic fluids trapped in fluid inclusions. Geochimica et Cosmochimica Acta 63, 3781–3797.
Burnham, C.W., 1997. Magmas and hydrothermal fluids, In: Barnes, H.L. (Ed.), Geochemistry of Hydrothermal Ore Deposits, Third Edition. Wiley, New York, pp. 63–123.
Carten, R.B., White, W.H., Stein, H.J., 1993. High-grade granite-related molybdenum systems: classification and origin. In: Kirkham, R.V., Sinclair, W.D., Thorpe, R.I., Duke, J.M. (Eds.), Mineral Deposits Modelling: Geological Association of Canada, Special Paper, 40, pp. 521–554.
Chakhmouradian, A.R., 2006. High-field-strength elements in carbonatitic rocks: geochemistry, crystal chemistry and significance for constraining the sources of carbonatites. Chemical Geology 235, 138–160.
Chakhmouradian, A.R., Mitchell, R.H., 1998. Lueshite, pyrochlore and monazite-(Ce) from apatite–dolomite carbonatite, Lesnaya Varaka complex, Kola Peninsula, Russia. Mineralogical Magazine 62, 769–782.
Chakhmouradian, A.R., Mitchell, R.H., 1999. Niobian ilmenite, hydroxylapatite and sulfatian monazite: alternative hosts for incompatible elements in calcite kimberlite at Internatsional'naya, Yakutia. The Canadian Mineralogist 37, 1177–1189.
Chakhmouradian, A.R., Mumin, A.H., Demény, A., Elliott, B., 2008. Postorogenic carbonatites at Eden Lake, Trans-Hudson Orogen (northern Manitoba, Canada): geological setting, mineralogy and geochemistry. Lithos 103, 503–526.
Chen, Y.J., Li, C., Zhang, J., Li, Z., Wang, H.H., 2000. Sr and O isotopic characteristics of porphyries in the Qinling molybdenum deposit belt and their implication to genetic mechanism and type. Science in China (Series D) 43 (Supp.), 82–94.
Costanzo, A., Moore, K.R., Wall, F., Feely, M., 2006. Fluid inclusions in apatite from Jacupiranga calcite carbonatites: evidence for a fluid-stratified carbonatite magma chamber. Lithos 91, 208–228.
Demény, A., Ahijado, A., Casillas, R., Vennemann, T.W., 1998. Crustal contamination and fluid/rock interaction in the carbonatites of Fuerteventura Canary Islands, Spain: a C, O, H isotope study. Lithos 44, 101–115.
Demény, A., Sitnikova, M.A., Karchevsky, P.I., 2004. Stable C and O isotope compositions of carbonatite complexes of the Kola Alkaline Province: phoscorite–carbonatite relationships and source compositions. In: Wall, F., Zaitsev, A.N. (Eds.), Phoscorites and Carbonatites from Mantle to Mine: The Key Example of the Kola Alkaline Province: Mineralogical Society, London, pp. 407–431.
Doroshkevich, A.G., Ripp, G.S., Viladkar, S.G., Vladykin, N.V., 2008. The Arshan REE carbonatites, southwestern Transbaikalia, Russia: mineralogy, paragenesis and evolution. The Canadian Mineralogist 46, 807–823.
Eby, G.N., 1975. Abundance and distribution of the rare-earth elements and yttrium in the rocks and minerals of the Oka carbonatite complex, Quebec. Geochimica et Cosmochimica Acta 39, 597–620.
Gao, S., Zhang, B.R., Li, Z.J., Wang, D.P., Ouyang, J.P., Xie, Q.L., 1996. Geochemical evidence for Proterozoic tectonic evolution of the Qinling Orogenic Belt and its adjacent margins of North China and Yangtze Cratons. Precambrian Research 80, 23–48.
Gao, S., Luo, T.C., Zhang, B.R., Zhang, H.F., Han, Y.W., Zhao, Z.D., Hu, Y.K., 1998. Chemical composition of the continental crust as revealed by studies in East China. Geochimica et Cosmochimica Acta 62, 1959–1975.
Geological Team no. 13 of the Shanxi Geological Bureau, 1989. A Detailed Geological Report on the Huanglongpu Mo Ore Area in Luona, Shanxi Province (in Chinese).
Hacker, B.R., Ratschbacher, L., Liou, J.G., 2004. Subduction, collision and exhumation in the ultrahigh-pressure Qinling–Dabie orogen. Geological Society (London) Special Publications 226, 157–175.
Hornig-Kjarsgaard, I., 1998. Rare earth elements in sovitic carbonatites and their mineral phases. Journal of Petrology 39, 2105–2121.
Hu, S.X., Lin, Q.L., Chen, Z.M., 1988. The geology and metallogeny of the amalgamation zone between ancient North China plate and South China plate. Nanjing University Press, Nanjing. (in Chinese).
Huang, D.H., Wu, C.Y., Du, A.D., He, H.L., 1995. Re–Os isotope ages of molybdenum deposits in East Qinling and their significance. Chinese Journal of Geochemistry 14, 313–322.
Keller, J., Hoefs, J., 1995. Stable isotope characteristics of recent natrocarbonatites from Oldoinyo Lengai. In: Bell, K., Keller, J. (Eds.), Carbonatites Volcanism: Oldoinyo Lengai and Petrogenesis of Natrocarbonatites. LAVCEI Proceeding in Volcanology. Springer-Verlag, Berlin, pp. 113–123.
Klemm, L.M., Pettke, T., Heinrich, C.A., 2008. Fluid and source magma evolution of the Questa porphyry Mo deposit, New Mexico, USA. Mineralium Deposita 43, 533–552.
Kretz, R., 1983. Symbols for rock-forming minerals. American Mineralogist 68, 277–279.
Kröner, A., Compston, W., Zhang, G.W., Guo, A.L., Todt, W., 1988. Age and tectonic setting of Late Archean greenstone-gneiss terrain in Henan Province, China, as revealed by single-grain zircon dating. Geology 16, 211–215.
Landtwing, M.R., Pettke, T., Halter, W.E., Heinrich, C.A., Redmond, P.B., Einaudi, M.T., Kunze, K., 2005. Copper deposition during quartz dissolution by cooling magmatic–hydrothermal fluids: the Bingham porphyry. Earth and Planetary Science Letters 235, 229–243.
Le Bas, M.J., Ba-bttat, M.A.O., Taylor, A.N., Milton, A.J., Windley, B.F., Evins, P.M., 2004. The carbonatite–marble dykes of Abyan Province, Yemen Republic: the mixing of mantle and crustal carbonate materials revealed by isotope and trace element analysis. Mineralogy and Petrology 82, 105–135.
Lehmann, B., 1987. Molybdenum distribution in Precambrian rocks of the Colorado Mineral Belt. Mineralium Deposita 22, 47–52.
Lehmann, B., 1988. Reply on the comment by Holly J. Stein and Judith L. Hannah on: Molybdenum distribution in Precambrian rocks of the Colorado Mineral Belt. Mineralium Deposita 23, 224–226.
Li, N., Chen, Y.J., Zhang, H., Zhao, T.P., Deng, X.H., Wang, Y., Ni, Z.Y., 2007. Molybdenum deposits in East Qinling. Earth Science Frontiers 14, 186–198 (in Chinese with English abstract).
Liang, Q., Hu, J., Gregoire, D.C., 2000. Determination of trace elements in granites by inductively coupled plasma mass spectrometry. Talanta 51, 507–513.
Mao, J.W., Zhang, Z.C., Zhang, Z.H., Du, A.D., 1999. Re–Os isotopic dating of molybdenites in the Xiaoliugou W–(Mo) deposit in the northern Qulian Mountains and its geological significance. Geochimica et Cosmochimica Acta 63, 1815–1818.
Mao, J.W., Xie, G.Q., Bierlein, F., Qu, W.J., Du, A.D., Ye, H.S., Pirajno, F., Li, H.M., Guo, B.J., Lie, Y.F., Yang, Z.Q., 2008. Tectonic implications from Re–Os dating of Mesozoic molybdenum deposits in the East Qinling–Dabie orogenic belt. Geochimica et Cosmochimica Acta 72, 4607–4626.
McDonough, W.F., Sun, S.S., 1995. The composition of the Earth. Chemical Geology 120, 223–253.
Meng, Q.R., Zhang, G.W., 2000. Geologic framework and tectonic evolution of the Qinling orogen, central China. Tectonophysics 323, 183–196.
Misra, K.C., 1999. Understanding Mineral Deposits. Kluwer Academic Publishers, Dordrecht. 845 pp.
Nelson, D.R., Chivas, A.R., Chappell, B.W., McCulloch, M.T., 1988. Geochemical and isotopic systematic in carbonatites and implications for the evolution of ocean–island sources. Geochimica et Cosmochimica Acta 52, 1–17.
Pouchou, J.L., Pichoir, F., 1984. A new model for quantitative analysis. I. Application to the analysis of homogeneous samples. La Récherche Aérospatiale 3, 13–38.
Ratschbacher, L., Hacker, B.R., Calvert, A., Webb, L.E., Grimmer, J.C., McWilliams, M.O., Ireland, T., Dong, S.W., Hu, J.M., 2003. Tectonic of the Qinling (Central China): tectonostratigraphy, geochronology, and deformation history. Tectonophysics 366, 1–53.
Reguir, E.P., 2001. Aspects of the Mineralogy of the Murun Alkaline Complex, Yakutia, Russia. Unpublished MSc Thesis, Lakehead University, Canada, 193 pp.
Reguir, E.P., Mitchell, R.H., 2000. The mineralogy of carbonatites and related potassic syenites from the Rocky Boy stock, Bearpaw Mountains, north-central Montana. GeoCanada 2000 Conference CD (extended abstracts), file 374 pdf.
Rusk, B.G., Reed, M.H., 2002. Scanning electron microscope-cathodoluminescence of quartz reveals complex growth histories in veins from the Butte porphyry copper deposit, Montana. Geology 30, 727–730.
Rusk, B., Reed, M., Dilles, J.H., Klemm, L., Heinrich, C.A., 2004. Compositions of magmatic hydrothermal fluids determined by LA–ICP–MS of fluid inclusions from the porphyry copper–molybdenum deposit at Butte, Montana. Chemical Geology 210, 173–199.
Rusk, B.G., Reed, M.H., Dilles, J.H., 2008. Fluid inclusion evidence for agmatic–hydrothermal fluid evolution in the porphyry copper–molybdenite deposit at Butte, Montana. Economic Geology 103, 307–334.
Seedorff, E., Einaudi, M.T., 2004a. Henderson porphyry molybdenum system, Colorado: II. Decoupling of introduction and deposition of metals during geochemical evolution of hydrothermal fluids. Economic Geology 99, 37–70.
Seedorff, E., Einaudi, M.T., 2004b. Henderson porphyry molybdenum system, Colorado: I. Sequence and abundance of hydrothermal mineral assemblages, flow paths of evolving fluids, and evolutionary style. Economic Geology 99, 3–35.
Seedorff, E., Dilles, J.H., Proffett, J.M., Einaudi, M.T., Zurcher, L., Stavast, W.J.A., Johnson, D.A., Barton, M.D., 2005. Porphyry Deposits: Characteristics and Origin of Hypogene Features: Economic Geology 100th Anniversary Volume, pp. 251–298.
Seedorff, E., Barton, M.D., Stavast, W.J.A., Maher, D.J., 2008. Root zones of porphyry systems: extending the porphyry model to depth. Economic Geology 103, 939–956.
Simon, A.C., Pettke, T., Candela, P.A., Piccoli, P.M., Heinrich, C., 2006. Copper partitioning in a melt–vapor–brine–magnetite–pyrrhotite assemblage. Geochimica et Cosmochimica Acta 70, 5583–5600.
Smith, M.P., Henderson, P., Campbell, L.S., 2000. Fractionation of the REE during hydrothermal processes: constraints from the Bayan Obo Fe–REE–Nb deposit, Inner Mongolia, China. Geochimica et Cosmochimica Acta 64, 3141–3160.
Stein, H.J., Hannah, J.L., 1988. Comment on the paper by Bernd Lehmann: molybdenum distribution in Precambrian rocks of the Colorado Mineral Belt. Mineralium Deposita 23, 222–223.
Stein, H.J., Markey, R.J., Morgan, J.W., Hannah, J.L., Schersten, A., 1997. Highly precise and accurate Re–Os ages for molybdenite from the East Qinling–Dabie molybdenum belt, Shanxi province, China. Economic Geology 92, 827–835.
Stein, H.J., Markey, R.J., Morgan, J.W., Hannah, J.L., Schersten, A., 2001. The remarkable Re–Os chronometer in molybdenite: how and why it works. Terra Nova 13, 479–486.
Sun, D.Z., Li, H.M., Lin, Y.X., Zhou, H.E., Zhao, E.Q., Tang, M., 1991. Precambrian geochronology, chronotectonic framework and model of chronocrustal structure of the Zhongtiao Mountains. Acta Geology Sinica 3, 216–231 (in Chinese, with English abstract).
Sun, W.D., Arculus, R.J., Bennett, V.C., Eggins, S.M., Binns, R.A., 2003. Evidence for rhenium enrichment in the mantle wedge from submarine arc-like volcanic glasses (Papua New Guinea). Geology 31, 845–848.
Tucker, M.E., Wright, V.P., 1990. Carbonate Sedimentology. Blackwell Scientific Publications, Oxford.
Ulrich, T., Mavrogenes, J., 2008. An experimental study of the solubility of molybdenum in H_2O and KCl–H_2O solutions from 500 °C to 800 °C, and 150 to 300 MPa. Geochimica et Cosmochimica Acta 72, 2316–2330.
Veizer, J., Plumb, K.A., Clayton, R.N., Hinton, R.W., Grotzinger, J.P., 1992. Geochemistry of Precambrian carbonates: V. Late Paleoproterozoic seawater. Geochimica et Cosmochimica Acta 56, 2487–2501.
Verwoerd, W.J., Viljoen, E.A., Chevallier, L., 1995. Rare metal mineralization at the Salpeterkop carbonatite complex, Western Cape Province, South Africa. Journal of African Earth Sciences 21, 171–186.

Villeneuve, M., Whalen, J.B., Anderson, R.G., Struik, L.C., 2001. The Endako batholiths: episodic plutonism culminating in the formation of the Endako porphyry molybdenite deposit, north-central British Columbia. Economic Geology 96, 171–196.
Wall, F., Zaitsev, A.N., 2004. Rare earth minerals in Kola carbonatites. In: Wall, F., Zaitsev, A.N. (Eds.), Phoscorites and Carbonatites from Mantle to Mine: The Key Example of the Kola Alkaline Province: Mineralogical Society, London, pp. 341–373.
Wall, F., Niku-Paavola, V.N., Storey, C., Müller, A., Jeffries, T., 2008. Xenotime-(Y) from carbonatite dykes at Lofdal, Namibia: unusually low LREE:HREE ratio in carbonatite, and the first dating of xenotime overgrowths on zircon. Canadian Mineralogist 46, 861–877.
Wedepohl, K.H., 1995. The composition of the continental crust. Geochimica et Cosmochimica Acta 59, 1217–1232.
Westra, G., Keith, S.B., 1981. Classification and genesis of stockwork molybdenum deposits. Economic Geology 76, 844–873.
Williams-Jones, A.E., Palmer, D.A.S., 2002. The evolution of aqueous-carbonic fluids in the Amba Dongar carbonatite, India: implications for fenitisation. Chemical Geology 185, 283–301.
Woolley, A.R., Kempe, D.R.C., 1989. Carbonatites: nomenclature, average chemical composition. In: Bell, K. (Ed.), Carbonatites: Genesis and Evolution. Unwin Hyman, London, pp. 1–14.
Xu, Z.W., Yang, R.Y., Liu, H.Y., Lu, X.C., Xu, W.Y., Ren, Q.J., 1998. Study on the ore-forming fluid of the Jinduicheng porphyry molybdenum deposit. Shanxi Province. Geological Journal of China Universities 4, 423–431 (in Chinese with English abstract).
Xu, C., Campbell, I.H., Allen, C.M., Huang, Z.L., Qi, L., Zhang, H., Zhang, G.S., 2007. Flat rare earth element patterns as an indicator of cumulate processes in the Lesser Qinling carbonatites, China. Lithos 95, 267–278.
Xu, C., Campbell, I.H., Kynicky, J., Allen, C.M., Chen, Y.J., Huang, Z.L., Qi, L., 2008. Comparison of the Daluxiang and Maoniuping carbonatitic REE deposits with Bayan Obo REE deposit, China. Lithos 106, 12–24.
Xue, F., Lerch, M.F., Kröner, A., Reischmann, T., 1996. Tectonic evolution of the East Qinling Mountains, China, in the Paleozoic: a review and new tectonic model. Tectonophysics 253, 271–284.
Yang, X.M., Le Bas, M.J., 2004. Chemical compositions of carbonate minerals from Bayan Obo, Inner Mongolia, China: implications for petrogenesis. Lithos 72, 97–116.
Zhang, B.R., Luo, T.C., Gao, S., Ouyang, J.P., Chert, D.X., Ma, Z.D., Han, Y.W., Gu, X.M., 1994. A Geochemical Study of Lithosphere, Tectonic Evolution and Metallogenesis of East Qinling and its Adjacent Regions. China University of Geosciences Press, Wuhan. (in Chinese with English abstract).
Zhang, Z.W., Yang, X.Y., Dong, Y., Zhu, B.Q., Chen, D.F., in press. Molybdenum deposits in the eastern Qinling, central China: constraints on the geodynamics. International Geology Review. doi:10.1080/00206810903053902